Mon. Not. R. Astron. Soc. **000**, 000–000 (0000) Printed 14 February 2017 (MN LATEX style file v2.2)

On-sky demonstration of matched filters for wavefront measurements using ELT-scale elongated laser guide stars

A. G. Basden[1⋆], L. Bardou[2], D. Bonaccini Calia[3], T. Buey[2], M. Centrone[4], F. Chemla[5], J. L. Gach[6], E. Gendron[2], D. Gratadour[2], I. Guidolin[3], D. R. Jenkins[1], E. Marchetti[3], T. J. Morris[1], R. M. Myers[1], J. Osborn[1], A. P. Reeves[1], M. Reyes[7], G. Rousset[2], G. Lombardi[8], M. J. Townson[1], F. Vidal[2],

[1] *Department of Physics, Durham University, South Road, Durham, DH1 3LE, UK*
[2] *LESIA, Observatoire de Paris - Paris Sciences et Lettres, CNRS, Université P. et M. Curie - Sorbonne Universités, Université Paris Diderot - Sorbonne Paris Cité, 5, Place Jules Janssen, 92190 Meudon, France*
[3] *European Southern Observatory, Garching, Germany*
[4] *INAF - Instituto Nazionale de Astrofisica, Observatorio Astronomico di Roma, Via Frascati 33, 00078, Monte Porzio Catone (RM), Italy*
[5] *GEPI, Observatoire de Paris - Paris Sciences et Lettres, CNRS, Université Paris Diderot - Sorbonne Paris Cité, 5, Place Jules Janssen, 92190 Meudon, France*
[6] *Laboratoire dAstrophysique de Marseille, 38 rue F. Joliot-Curie, 13388 Marseille Cedex 13, France*
[7] *Instituto de Astrofisica de Canarias, Via Lactea, La Laguna, Tenerife, Spain*
[8] *Gran Telescopio Canarias, Cuesta de San Jos, s/n - E-38712, Brea Baja, La Palma, Spain*

arXiv:1702.03736v1 [astro-ph.IM] 13 Feb 2017

14 February 2017

ABSTRACT

The performance of adaptive optics systems is partially dependant on the algorithms used within the real-time control system to compute wavefront slope measurements. We demonstrate use of a matched filter algorithm for the processing of elongated laser guide star (LGS) Shack-Hartmann images, using the CANARY adaptive optics instrument on the 4.2 m William Herschel Telescope and the European Southern Observatory Wendelstein LGS Unit placed 40m away. This algorithm has been selected for use with the forthcoming Thirty Meter Telescope, but until now had not been demonstrated on-sky. From the results of a first observing run, we show that the use of matched filtering improves our adaptive optics system performance, with increases in on-sky H-band Strehl measured up to about a factor of 1.1 with respect to a conventional centre of gravity approach. We describe the algorithm used, and the methods that we implemented to enable on-sky demonstration.

Key words: Instrumentation: adaptive optics, laser guide stars Methods: numerical

1 INTRODUCTION

Adaptive optics (AO) systems have reached a new level of maturity in recent years, with many new strategies and algorithms being demonstrated and realised in facility class systems, e.g. eXtreme AO (XAO) (Fusco et al. 2006; Jovanovic et al. 2015; Macintosh et al. 2012) and multi-conjugate adaptive optics (MCAO) (Rigaut et al. 2012). Future systems for the forthcoming Extremely Large Telescopes (ELTs) are currently under development, and it is important that optimum performance is obtained for these expensive facilities. A key area of investigation is optimisation of algorithms that are used in the AO real-time pipeline, to extract maximum information from the photons received by the wavefront sensors (WFSs), and using *apriori* knowledge of the atmosphere to compute the best match of deformable mirror (DM) surface to the phase perturbations introduced by atmospheric turbulence.

In order to increase sky coverage of AO corrected observations (which are limited by the availability of bright natural guide stars), laser guide stars (LGSs) are used (Foy & Labeyrie 1985). Artificial stars can be created in the mesosphere, at about 90 km above the surface of the Earth, using a laser tuned to the resonance of sodium atoms. However, due to the thickness of the sodium layer, this leads to an elongation of the spots in a Shack-Hartmann

⋆ E-mail: a.g.basden@durham.ac.uk (AGB)

© 0000 RAS

WFS when sub-apertures view the LGS off-axis, due to perspective (Gilles & Ellerbroek 2006). This elongation is approximately proportional to the distance between the sub-aperture (projected onto the telescope pupil) and the laser launch location (projected into the plane of the primary mirror). For the European ELT (E-ELT), this distance can reach about 40 m (Tamai & Spyromilio 2014) (for a small number of most affected sub-aperture), and so spots extend for up to 20–30 arcseconds along the elongation direction, depending on the precise distribution of mesospheric sodium atoms. Spots that are this large introduce several challenges for wavefront sensing: flux is spread over a larger number of pixels and so signal to noise ratio (SNR) is reduced, and sensitivity to spot motion along and perpendicular to the elongation direction differs.

Here, we consider the use of a noise-optimal matched filter algorithm (Gilles & Ellerbroek 2006, 2008; Conan et al. 2009) for calculation of local wavefront gradients in a Shack-Hartmann WFS. We report on successful on-sky operation of this algorithm, taking advantage of a dedicated experiment set to evaluate the performance of AO using ELT-scale elongated LGSs (Rousset et al. 2014). This experiment is based on the use of the CANARY AO technology demonstrator instrument (Myers et al. 2008; Gendron et al. 2011) at the 4.2 m William Herschel Telescope coupled to the European Southern Observatory (ESO) Wendelstein LGS Unit (WLGSU) (Bonaccini Calia et al. 2012) with the laser being launched 40 m away from the WHT. Performance of the AO system when using the matched filter algorithm is compared with that obtained using a well optimised centre of gravity (COG) approach (see §3.3.2 for further details about the optimisation). The matched filter algorithm has been selected for use with the forthcoming Thirty Meter Telescope (Nelson & Sanders 2008), and, as we show, also has relevance for other telescopes. Previous authors have also compared the performance of different algorithms used for wavefront slope determination for Shack-Hartmann WFSs (Thomas et al. 2006; Basden et al. 2015). Here we provide results of the first on-sky verification of one of these.

The CANARY AO system has seen several phases of operation using many different WFSs and DMs (Basden et al. 2016). Here, we operate in phase D mode (Rousset et al. 2014), with a single on-axis sodium LGS, an on-axis natural guide star (NGS) truth WFS, and optionally, three off-axis NGSs (which we do not consider further here). Phase D of CANARY is designed to emulate a sub-pupil of the E-ELT, with the LGSs being launched far off axis so that significant spot elongation effects can be studied. The WFSs all have 7×7 sub-apertures, of which 36 are valid (not significantly vignetted). The LGS WFS has 30×30 pixels per sub-aperture, and is based on an electron multiplying CCD (EMCCD) detector with sub-electron readout noise (Gach et al. 2016). It is equipped with a dedicated fast steering mirror to stabilize the LGS spots in the subapertures. Wavefront correction is performed using an 8×8 actuator DM with 52 active actuators and a dedicated tip/tilt mirror.

We concentrate our efforts on matched filtering of highly elongated sodium LGS spots, as shown in Fig. 1, though we have also tested with NGS spot patterns. However, on-sky observing time was limited and so we do not present results for NGSs: we did not take comprehensive NGS measurements once the AO loop was successfully closed.

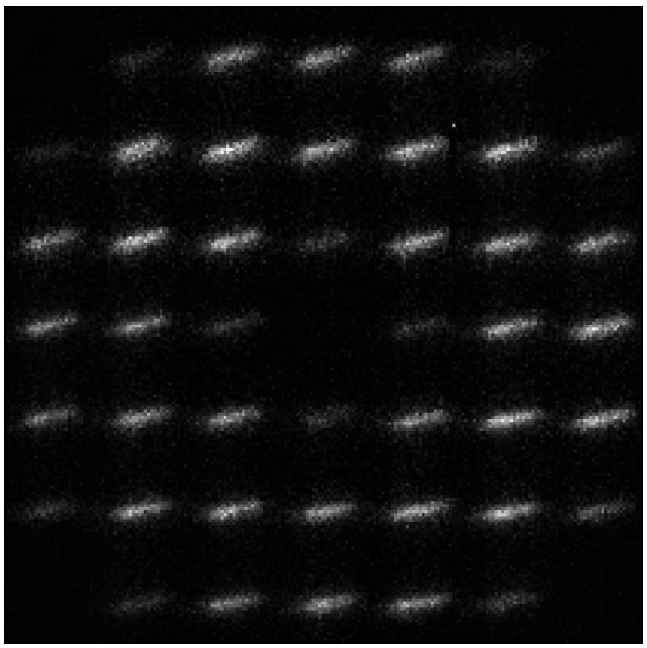

Figure 1. A figure showing a single WFS frame of elongated laser guide star spots recorded by the CANARY AO system on 20^{th} September 2016. This image has 30×30 pixels per sub-aperture, and a pixel scale of 0.65 arcseconds per pixel.

The matched filter algorithm has been developed to help mitigate some of the problems introduced by guide star elongation, including reduction in flux per pixel and sensitivity loss due to structure. Previous studies, e.g. Gilles & Ellerbroek (2006) have found that spot position estimation error is significantly impacted by this elongation, and that using a matched filter can reduce this effect, particularly in the presence of low photon signal and high detector readout noise.

Unfortunately, the matched filter algorithm is non-linear, i.e. estimated position and hence root-mean-square (RMS) error depend non-linearly on distance of the spot from the reference position of the matched filter. However, a linearity extension has been proposed (Gilles & Ellerbroek 2008) which we use to extend the linearity of this algorithm up to about 1 pixel of displacement. Additionally, because we operate in closed loop (as with the Thirty Metre Telescope (TMT)), the AO system helps to maintain the spots in a central position, though we note that spot motion can still be large for wide-field LGS systems and ground layer AO (GLAO) systems. The pixel scale of the WFS that we use is also fairly large, at 0.65 arcseconds per pixel, principally so that a reasonable sub-aperture size can have sufficient field of view to image the entire LGS spot, and therefore, under reasonable seeing conditions (e.g. 0.7 arcseconds), LGS spot motion is small, within the linear range of the matched filter algorithm.

In the case of the forthcoming E-ELT, laser guide stars are launched from the edge of the telescope pupil, and so the degree of elongation varies across a Shack-Hartmann WFS from close to zero (for sub-apertures near the launch location) to about 40 m (for sub-apertures furthest from the launch location), which corresponds to tens of arcseconds of angular diameter for typical sodium layer profiles and

thickness. In this case, a COG algorithm can be expected to perform well for sub-apertures with little elongation, and poorly for well elongated sub-spertures. The matched filter algorithm is able to improve measurement accuracy for all sub-apertures, with the largest gain being for those that are most elongated.

In §2 we describe the technique that we use to build and apply the matched filters. In §3 we present on-sky results, and we conclude in §4.

2 MATCHED FILTERS FOR WAVEFRONT GRADIENT ESTIMATION

We follow the derivation of the matched filter as given by Gilles & Ellerbroek (2006), with an extension for dynamic range (Gilles & Ellerbroek 2008). This is outlined as follows.

The sub-aperture pixel intensity is modelled as:

$$I_m(\vec{x}) = I_0(\vec{x}) + G \cdot \vec{x} + \eta \tag{1}$$

where I_m is the intensity of a pixel at location $\vec{x}$, I_0 is the high light level on-axis intensity (assumed to be noiseless), G is the derivative of I_0 in the x and y directions (the pixel gain, or Jacobian) having components G_x and G_y, and η is the measurement noise vector due to the photon shot noise and detector readout noise.

The minimisation of the difference between measured pixel intensity and model pixel intensity (Eq. 1 is required to compute the estimate of the spot location, and the derivation is given by Gilles & Ellerbroek (2008). In summary (with small modifications made by us to allow for variations in flux measurements), estimated spot position is given by

$$\vec{s_x} = \frac{R \cdot I}{\sum I} \tag{2}$$

where $\vec{s_x}$ is the desired slope measurement, I is the sub-aperture image (flattened into a one-dimensional array) and $\sum I$ is a measure of the total flux within I. R (the matched filter), which has both x and y components is given by

$$R = fM(H^T C^{-1} H)^{-1} H^T C^{-1} \tag{3}$$

with C being the noise covariance matrix (a diagonal matrix of side length equal to the number of pixels within a sub-aperture), with entries equal to $I_0 + \sigma^2$ for photon and detector noise where σ is the detector readout noise, f is the sum of flux in I_0,

$$M = \begin{bmatrix} 1 & 0 & 0 & 1 & -1 & 0 & 0 \\ 0 & 1 & 0 & 0 & 0 & 1 & -1 \end{bmatrix} \tag{4}$$

and

$$H = \begin{bmatrix} G_x & G_y & I_0 & I_1 & I_2 & I_3 & I_4 \end{bmatrix} \tag{5}$$

Here, $I_{1,2,3,4}$ are the high light level intensities of the spot, shifted in the +x, -x, +y and -y directions respectively by one pixel.

2.1 Calculation of the matched filter

Ideally, calculation of the matched filter would be an ongoing process, continually computed by dithering of the LGS spots on the WFS, using a tip-tilt mirror (Gilles & Ellerbroek 2006), to allow ongoing calculation of the image gradients, G_x and G_y. Dithering would have little effect on the AO correction since global LGS motion is ignored, being removed from the slope measurements before being passed to the reconstructor. Continual calculation means that the matched filter remains relevant over long periods while atmospheric conditions, and sodium layer profile change. The introduction of a small, known, time-varying astigmatism will enable continual calculation of the relative pixel scales of both the LGS and NGS WFSs (key to maintaining AO performance in varying seeing conditions). If the introduced astigmatism is kept small (and detected using a phase locked loop), effect on image point spread function (PSF) will be minimal.

However, since CANARY is an AO demonstrator, and does not need to produce astronomical science, and therefore does not require AO stability for long integration periods, we have taken the approach of building the matched filter off-line to simplify on-sky operation, which is used for all results presented here. We hope to develop an online calculation capability for future sky tests and operation.

Our sequence of operations to build the matched filter is as follows.

(i) The LGS fast steering mirror is set to dither, with four separate positions per cycle.

(ii) WFS slope measurements (using a COG) are recorded and used to determine the relative phase difference between the mirror and WFS. Since this is performed on averaged images, signal levels can be high, allowing the COG estimation to be accurate.

(iii) The phase of the dithering is adjusted so that the shift in WFS spots is aligned with the detector pixels and sub-apertures.

(iv) A number of WFS images are recorded, and those corresponding to each of the four dithered mirror locations are averaged together. Typically 5–10 seconds of images are recorded.

(v) The COG of these four averaged images is computed, to give the dither radius (in pixels).

(vi) The image gradient, G_x and G_y are computed from the difference of opposing pairs of images divided by the diameter of the dither (in pixels).

(vii) The dithering is removed, and typically 5–10 seconds of images are averaged together to obtain I_0. I_1, I_2, I_3 and I_4 are also computed.

(viii) The matched filter, R is then computed.

When computing the matched filter, we find that tuning the WFS noise level estimate, σ, can be used to improve performance, since this parameter acts to regularise part of the solution for R. We use a single value for σ rather than a separate one for each pixel, partly for simplicity, and also because for a CCD detector, this is typically constant. However we note that for a scientific CMOS (sCMOS) detector (or indeed a multi-port CCD detector) there may be performance improvements if a different value for each pixel can be used, i.e. less weight can be applied to noisier pixels.

Once the matched filter has been computed, it is uploaded to the real-time control system and matched filtering switched on. It is then necessary for us to measure reference slopes, which we do by averaging the computed wavefront slope measurements over a sufficient number of frames for wavefront turbulence to average out. Typically, we record for about 60 seconds. We note however that this method

of removing static wavefront offsets is impractical for larger telescope apertures, since the time to average turbulence greatly increases (Gordon et al. 2011).

2.2 Application of the matched filter

The CANARY instrument uses a central processing unit (CPU)-based real-time control system, the Durham AO real-time controller (DARC) (Basden et al. 2010) which provides the necessary flexibility to implement, develop and test new algorithms. Within the real-time control system, the matched filter is applied as follows:

(i) Sub-aperture flux is computed in units of analogue to digital units (not photons), i.e. the calibrated pixels are summed.
(ii) The dot product of R_x with the sub-aperture pixels (flattened into a vector) is computed, and the result divided by the sub-aperture flux to give the x slope estimate.
(iii) Similarly for the y slope estimate using R_y.

DARC has the ability to actively track Shack-Hartmann spots, i.e. the sub-aperture positions can follow the spots, such that the spots remain close to the centre of the sub-aperture, based on the location of the spot in the previous image frame. This therefore aids the linearity of the matched filter algorithm, since the matched filter will be applied to spots that are close to the sub-aperture centre. The alternative to this approach, which we do not explore, is a two-step algorithm, which initially estimates spot position with a COG algorithm, and then applies the matched filter to this. However, this introduces additional computational complexity.

Within DARC, we use a different matched filter for each sub-aperture, and internally, these are stored in an two-dimensional array where the location of the matched filter corresponds with the default sub-aperture position. Therefore we can apply matched filtering to sub-apertures of different sizes, and to different spot elongations across the pupil.

2.3 Development and testing of matched filters

To develop the real-time implementation of the matched filter algorithm, and to test the technique used to build the matched filter we employed two simulation concepts. First, we use Durham AO simulation platform (DASP) (Basden et al. 2007) to model a single sub-aperture with an extended laser guide star spot viewed through atmospheric turbulence. We use this simulation tool to build the matched filter as outlined in §2. We then generate a sequence of atmospherically propagated Shack-Hartmann spots, as shown in Fig. 2 and compare the COG and matched filter spot position estimators with the true known location (measured on a noiseless image using a COG). The RMS deviation of each estimator from the known position is then computed. We are able to explore matched filter performance covering a parameter space including elongation, signal level, readout noise level and number of frames used when building the matched filter. Although we do not seek to present significant simulated results here, because matched filter performance has been studied elsewhere, for example Conan et al. (2009),

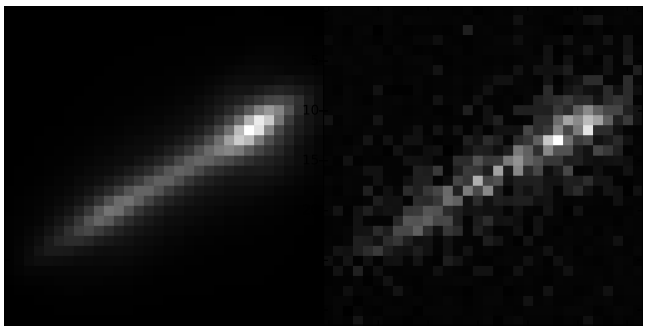

Figure 2. An example atmospherically propagated sodium LGS Shack-Hartmann spot, as used in simulations (6.4 arcsecond field of view). Left: Noiseless image. Right: With added photon show noise (for a total flux of 1000 photons) and readout noise (0.1 electrons per pixel RMS).

we present a summary of our modelling. This modelling is based on a LGS launched 40 m from the telescope aperture (approximating CANARY and furthest sub-apertures of the E-ELT), and a 60 cm sub-aperture. We note that for the TMT, which uses centre-launched LGSs, maximum sub-aperture distance from the launch axis will be about 15 m. Default photon flux in our simulations is 1000 photons per sub-aperture per frame (pessimistic compared with on-sky measurements by a factor of about 2–5, Bonaccini Calia 2016) with sub-electron readout noise (i.e. an electron multiplying CCD). Seeing of 1 arcsecond is assumed, and by default we use 1000 images to build the matched filters.

After verification of the matched filter algorithm, we proceeded to develop the real-time implementation and support tools. To verify the operation of these, we use the real-time simulation concept (Basden 2014) coupling a Monte-Carlo simulation tool (DASP) to the real-time control system used by CANARY. This concept is simple: instead of using real physical cameras and DMs, they are instead simulated, with the simulation WFS camera data being fed into the real-time control system. The DM command output is captured and used to shape simulated DMs. We are then able to use the user interface tools developed for on-sky operation with this simulated system, and therefore provide a thorough testing, significantly reducing necessary on-sky commissioning time. The real-time control system itself does not need to know whether it is operating with real or simulated cameras and DMs.

We note that since the CANARY real-time control system is CPU-based, we do not need to operate the real-time simulation facility on the same computational hardware, i.e. we can, for example, operate the simulation and real-time control system on a developer's PC, to aid development when not present at the telescope, and to allow multiple instances of the system to be run simultaneously.

By using this real-time simulation, we are then able to test building of the matched filter (including dithering), and application of the matched filter, including engaging the AO loop.

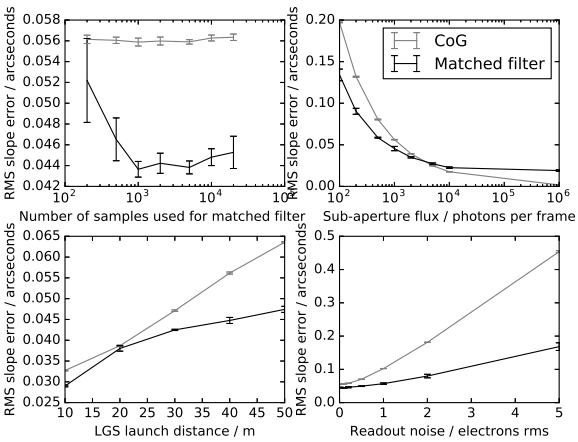
RMS slope error / arcseconds
Number of samples used for matched filter
CoG
Matched filter
Sub-aperture flux / photons per frame
LGS launch distance / m
Readout noise / electrons rms

Figure 3. A figure comparing matched filtering with COG. The sub-plots give performance as RMS estimation slope error (in arcseconds) with respect to a noiseless CoG measurement (lower error is better performance). These plots show performance (a) as a function of number of images used to build the matched filter, (b) as a function of guide star flux, (c) as a function of distance of the LGS from the telescope axis, and (d) as a function of detector readout noise.

3 MATCHED FILTERING RESULTS

We performed tests of matched filtering using the CANARY AO on-sky demonstrator instrument over a period of three nights in September 2016. During this operation, the WL-GSU launch telescope was set about 40 m from the William Herschel Telescope (WHT) to generate the sodium LGS in the mesosphere. Therefore, spots were highly elongated, as shown in Fig. 1.

3.1 Simulation measurements

Exploration of the matched filter parameter space was used to confirm the range of expected parameters over which matched filtering would out perform a COG algorithm. Fig. 3 shows some of these results that we obtained with simulation, and it can be seen (in agreement with previous studies) that matched filtering can yield improved performance when compared with COG. We note that at high light levels, the COG performs better since we are using a noiseless COG measurement as the "truth".

During AO operation, if the matched filter is to be updated, reference slopes will also require updating. Within simulation we developed a technique to compute updated reference slopes:

(i) Compute COG and matched filter measurements of the reference image, I_0, giving c_x, c_y, m_x, and m_y respectively, defined in pixels offset for the x and y directions.
(ii) Add the matched filter estimates, m_x and m_y, to the existing reference slopes.
(iii) Subtract the COG estimates, c_x and c_y, from the existing reference slopes.

If a matched filter is already in use, i.e. the matched filter is to be updated, an additional step is required, equal to the reverse of the above, i.e. adding the COG of the original image and subtracting the matched filter estimate of the original image. We note that a similar approach has been successfully taken for correlation wavefront sensing (Basden et al. 2014).

3.2 On-bench testing

We used the CANARY laboratory sky simulator (which uses LED light sources and two rotating phase screens to mimic the sky) to confirm that the matched filtering tools were operating as expected, dithering the sources, and building the matched filters. The WFS noise (due to shot noise and readout noise) was seen to be reduced by more than a factor of four (from 400 nm to 90 nm), reducing total wavefront error (in the first 36 Zernike modes) from 950 nm to 750 nm RMS, for the configuration in which it was used, confirming that the matched filter was working. To compute WFS noise, we compute noise variance of the wavefront slope measurements, and propagate this through a theoretical Zernike reconstruction matrix, and sum the first 36 terms, as is done by Vidal et al. (2014).

3.3 On-sky measurements

In this section, the on-sky performance is given in term of Strehl ratio as directly measured in the H-band infrared images recorded by the on-axis CANARY science camera. The AO loop is always closed on the on-axis elongated LGS for the high order correction while the tip and tilt correction is provided by the CANARY on-axis Truth WFS. The LGS slope estimation algorithm was alternated between COG and matched filtering.

The COG algorithm used as the reference for these performance comparisons was well optimised: we use the brightest pixel selection algorithm (Basden et al. 2012) to significantly reduce the effect of detector readout noise, with about 90 brightest pixels being selected, this number having been chosen for best performance, as shown in Fig. 4. In this case, the 90 brightest pixels are used for calculation of the COG, after a threshold equal to the value of the 91st pixel is applied. Reference slopes for both the COG and matched filter were measured on-sky, averaging 10000 frames of data (66 s) before using each algorithm.

3.3.1 16th September 2016

Initial on-sky measurements were taken on the night beginning on 16th September 2016. The LGS was elongated to about 13 arcseconds as measured by the WFS, and the elongation was aligned with the horizontal axis of the WFS. The amplitude of the LGS dither was set to 0.1 arcseconds diameter, and 1000 frames of data were used (250 at each dither location) during recording of the image gradient, G, and a separate 1000 frames used to measure I_0 (without dithering). The frame rate was 150 Hz, so 1.6 s of data was recorded for each dither location.

These results were measured close to dawn, when sky background was increasing. Eventually, the NGS tip-tilt signal was insufficient to provide good correction, so we did not record further data. We interleaved COG and matched filter measurements.

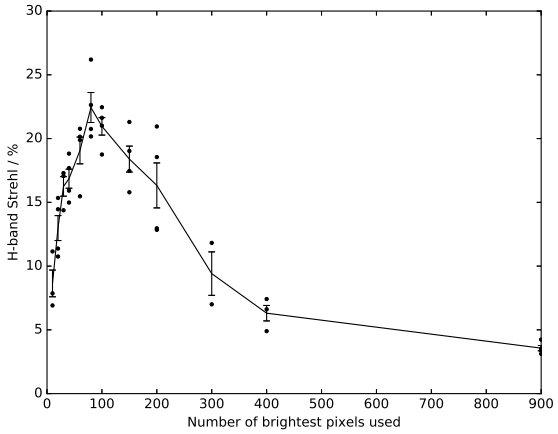

Figure 4. A figure showing AO performance as a function of number of brightest pixels chosen for the LGS WFS when using a COG algorithm. Closed-loop H-band Strehl ratio is shown, with the LGS used for high order correction, and an on-axis NGS for tip-tilt correction. The line with error bars is the standard deviation computed from the available information (shown) for each number of pixels. The LGS had about 13 arcseconds of elongation.

A single matched filter was used that for the duration of the experiment on this night. The matched filter computed from the data is shown in Fig. 5, along with the components used to make it, I_0, G_x, and G_y. We note that a few streaks are seen in these images due to problems with detector voltage levels (currently being repaired).

Fig. 6 shows measured AO system performance with and without matched filtering. It should be noted that due to atmospheric variability, we interleave measurements, so that trends in seeing with time can be somewhat mitigated. We present these results as a function of r_0, which is computed from the average value computed using the pseudo-open-loop slope measurements from the three off-axis NGS wavefront sensors using standard CANARY tools (Vidal et al. 2014). It is evident that the matched filter is providing significantly better performance than the COG algorithm.

3.3.2 17th September 2016

Further investigation of matched filtering performance was carried out, with the LGS spots elongated to about 13 arcseconds, at an angle of about 10 degrees from the horizontal axis of the WFS. This time, the matched filter was built using a reference image (I_0) that was computed while dithering, using a shift-and-add of the Shack-Hartmann images, based on the COG of the spots.

Strehl ratio was recorded using the CANARY infrared camera, at H-band, and Fig. 7 shows these results. There is significant scatter due to variable seeing conditions. However, matched filtering can be seen to deliver performance improvements compared to COG, increasing the mean Strehl ratio by a factor of greater than 1.1.

Dither amplitude	Matched filter Strehl / %	COG Strehl / %	Improvement
0.2 arcsec	16.6± 1.1	15.1±0.9	10%
0.1 arcsec	10.8±1.2	8.8±0.6	23%
0.05 arcsec	14.3± 0.7	14.2± 0.6	1%

Table 1. A table showing matched filter and COG performance for different dither amplitudes. The relative performance improvement when using matched filtering is also given.

3.3.3 19th September 2016

When building a matched filter, the dither amplitude used will affect performance. We therefore investigated three different dither amplitudes, setting it first to 0.2 arcseconds diameter, then to 0.1 arcseconds (as on previous nights) and finally to 0.05 arcseconds. Again, the LGS spots were elongated to about 13 arcseconds at an angle of about 10 degrees. In this case, the reference image, I_0 was obtained from averaging 1000 image frames without dithering (and without shift-and-add). As before, reference slopes were measured on-sky before the AO loop was closed for each matched filter and COG acquisition, in this case, with each dither amplitude.

Fig. 8 shows the AO performance obtained. Again it can be seen that the matched filter algorithm gives consistently better performance than the COG, except for the case with a dither amplitude of 0.05 arcseconds, where the performance gain is marginal. The COG and matched filter measurements are given as a function of Fried's parameter, r_0 so as to account for variable atmospheric seeing. We note that there is no algorithmic difference between the different CoG points in each figure, they were just recorded at different times (interleaved with the corresponding matched filter measurements), and hence different atmospheric conditions, using different sets of on-sky reference slopes. The mean matched filter measurements (table 1) show an improvement over the corresponding COG measurements, though we note that due to differing seeing, computing a mean Strehl ratio does not give an accurate performance estimate; rather it serves to give us a rough idea of relative performance. From these measurements, and from Fig. 8(c), it is evident that a dither of 0.05 arcseconds is too small for us to build a matched filter (this equates to 7% of a pixel).

3.3.4 On-sky results summary

We have explored matched filtering performance with E-ELT scale extended LGS Shack-Hartmann images over several nights of operation, and in each case, we have found that matched filtering leads to AO performance improvements when compared with COG.

We note that in our case, because all sub-apertures were well elongated, the gain in WFS performance using the matched filter was evident. For an ELT, with elongation varying more significantly across the WFS, the total performance gain may be smaller, though still significant. We also note that the LGS elongation was varying during the night and from night to night, following the sodium layer thickness variations (Moussaoui et al. 2010).

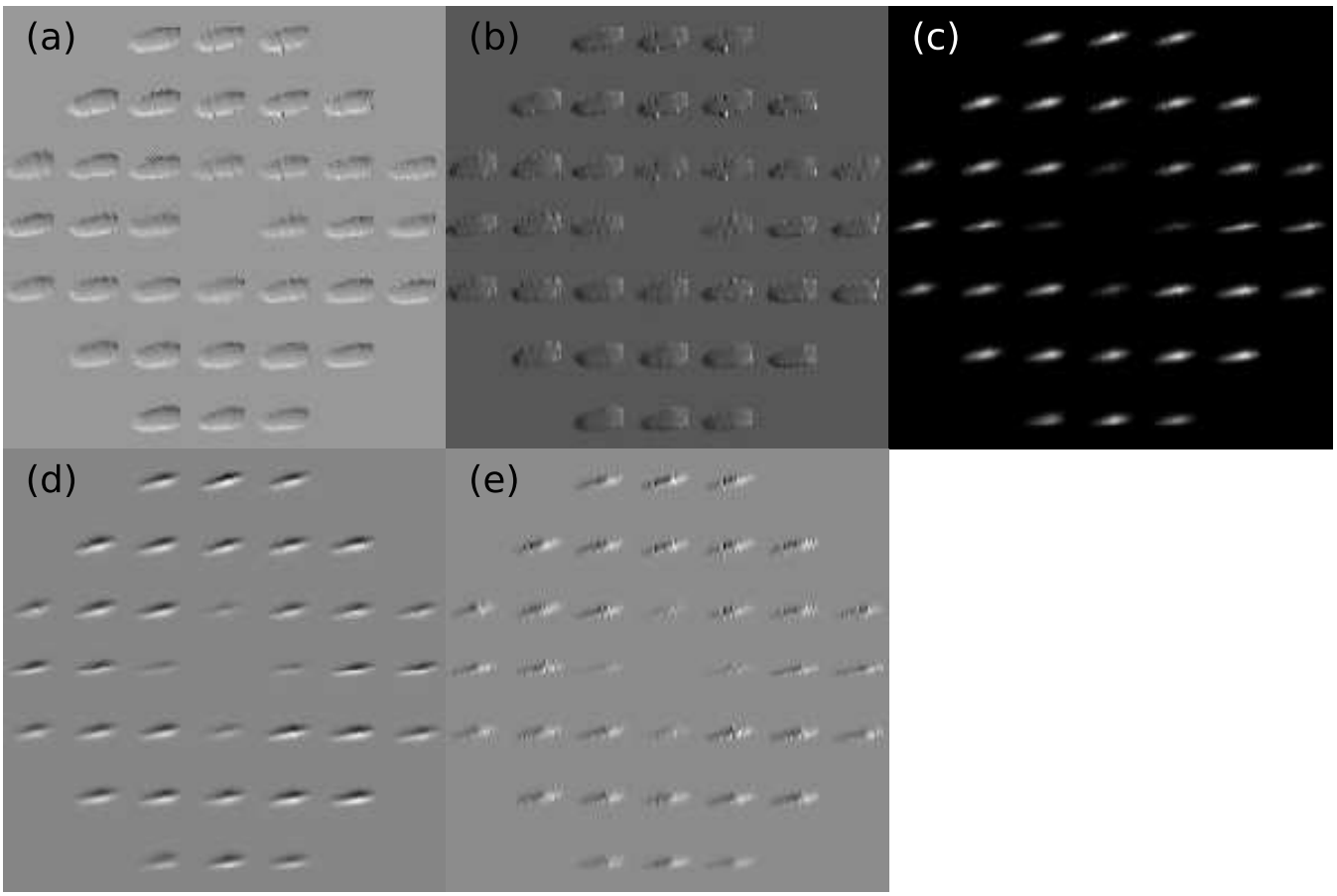

Figure 5. A figure showing, for the 7×7 sub-apertures of the CANARY phase D LGS, (a) an on-sky matched filter x component, (b) the matched filter y component, (c) I_0, (d) G_x, and (e) G_y. We note that we had some trouble with detector voltage levels, resulting in a few streaks in the image. This is manifested within the matched filter.

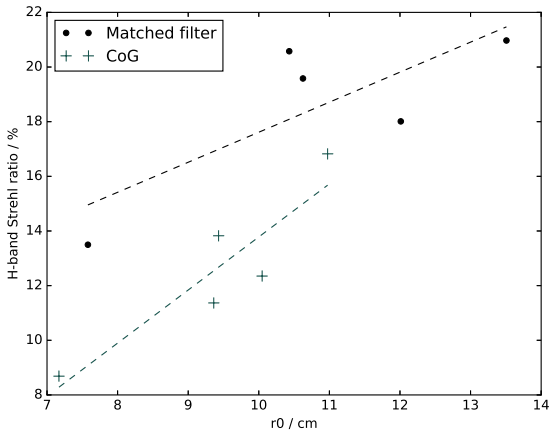

Figure 6. A figure showing H-band Strehl ratio for CoG and matched filtering measured on the night of 16th September. Data are plotted as a function of Fried's parameter, r_0, which is related to seeing. A 2 s exposure time is used for the science images, for a star with a V-band apparent magnitude of 9.47. The LGS WFS is recording approximately 3000 photons per sub-aperture per frame. The matched filter and corresponding reference slopes were recorded preceeding acquisition of the data.

3.4 Open-loop considerations

Our tests of matched filtering have been implemented using a closed-loop AO system, and so measured performance may be less affected by non-linearity effects than would be seen using an open-loop AO system, since the AO loop helps to maintain the Shack-Hartmann spots close to their reference positions. Therefore, performance with an open-loop AO system may not be so positive since spot motion will be larger, and spots may travel outside the linear range of the matched filter. In this case, either a two-step algorithm is required (using an initial COG estimate to find the approximate location to apply the matched filter to), or the use adaptive sub-aperture windowing allowing the sub-aperture to track the spot motion.

There are no proposed ELT instruments that are entirely open-loop: although the proposed MOSAIC instrument (Hammer et al. 2014) on the E-ELT has an open-loop multi-object AO (MOAO) system, it operates with a closed-loop GLAO correction, and therefore, a significant amount of spot motion will be mitigated (for likely atmospheric turbulence profiles, Sarazin et al. 2013; Osborn et al. 2010). Therefore matched filtering may still be appropriate here.

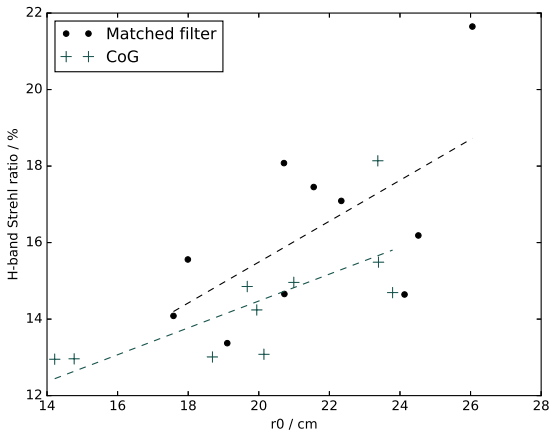

Figure 7. A figure showing H-band Strehl ratio as a function of Fried's parameter for the different centroiding modes measured on the night of 17th September. Black circles represent matched filtering, while crosses are for centre of gravity. Mean Strehl values are given in the legend. The same target was used as on the previous night.

3.5 Future work

Although we have demonstrated LGS AO operation of a matched filter algorithm on-sky, there remains further much work to do, which we will attempt during future CANARY on-sky observing runs. Building the matched filter during AO loop operation, and determination of pixel scale change, is essential to improve AO observational efficiency.

Additionally, successful implementation of on-line reference slope calculation is also necessary: for the measurements presented here, we compute reference slopes for the matched filter algorithm on-sky, by averaging many frames of slope measurements (typically 10000) to average atmospheric turbulence. These slopes are then added to the reference slopes required to correct non-common path aberrations. This method does not represent efficient use of telescope time unless slope measurements are monitored and updated continuously while in operation. Therefore a method to determine new matched filter reference slopes using the matched filter and initial reference slopes (either from a COG or previous matched filter) is required.

A further in-depth study of matched filter performance for different LGS sodium layer profiles and elongations is also necessary, with the improvements in wavefront error being calculated when the matched filter algorithm is used. Moreover we will compare the matched filtering algorithm with other slope estimation methods in greater depth. The comparison with other slope estimation methods requires a sufficient number of on-sky observations to be statistically meaningful, hence more observing time.

4 CONCLUSIONS

We have successfully implemented and demonstrated a noise-optimal matched filtering algorithm for determination of local wavefront gradients using a Shack-Hartmann sensor. On-sky testing was performed using the CANARY AO demonstrator instrument on the William Herschel Telescope together with the ESO Wendelstein laser guide star unit.

We find that matched filtering can deliver AO performance improvements compared with the conventional centre of gravity algorithm, and we measure improvements in H-band Strehl ratio of up to about 10% (i.e. the Strehl improves by a factor of 1.1).

We therefore conclude that a matched filtering algorithm is well suited for AO systems with elongated Shack-Hartmann spot patterns, providing better performance than the commonly used COG algorithm. Our demonstration represents a significant risk mitigation though further work is required. Direct comparison with other methods, such as correlation, also have to be tested.

ACKNOWLEDGEMENTS

This work is funded by the UK Science and Technology Facilities Council, grant ST/K003569/1, and a consolidated grant ST/L00075X/1. The ESO participation and installed infrastructure is funded under the ESO Technology Development Program. This work was partially supported by the European Commission (Fp7 Infrastructures 2012-1, OPTICON Grant 312430, WP1). This work is also supported by the European Southern Observatory. CANARY is a visitor instrument to the William Herschel Telescope, operated by the Isaac Newton Group in the Spanish Observatorio del Roque de los Muchachos of the Instituto de Astrofisica de Canarias.

REFERENCES

Basden A. G., 2014, MNRAS, 439, 2854
Basden A. G., Atkinson D., Bharmal N. A., Bitenc U., Brangier M., Buey T., Butterley T., et al. 2016, MNRAS, 459, 1350
Basden A. G., Butterley T., Myers R. M., Wilson R. W., 2007, Appl. Optics, 46, 1089
Basden A. G., Chemla F., Dipper N., Gendron E., Henry D., Morris T., Rousset G., Vidal F., 2014, MNRAS, 439, 968
Basden A. G., Geng D., Myers R., Younger E., 2010, Appl. Optics, 49, 6354
Basden A. G., Morris T. J., Gratadour D., Gendron E., 2015, MNRAS, 449, 3537
Basden A. G., Myers R. M., Gendron E., 2012, MNRAS, 419, 1628
Bonaccini Calia D., 2016, in Adaptive Optics Systems V Vol. 9909 of Society of Photo-Optical Instrumentation Engineers (SPIE) Conference Series, LGS return flux: report on the Tenerife optimization experiments and comparison with the Toptica laser results at the VLT. p. 9909
Bonaccini Calia D., Guidolin I., Friedenauer A., Hager M., Karpov V., Pfrommer T., Holzlöhner R., Lewis S., Hackenberg W., Lombardi G., Centrone M., Pedichini F., 2012, in Modern Technologies in Space- and Ground-based Telescopes and Instrumentation II Vol. 8450 of Society of Photo-Optical Instrumentation Engineers (SPIE) Conference Series, The ESO transportable LGS Unit for mea-

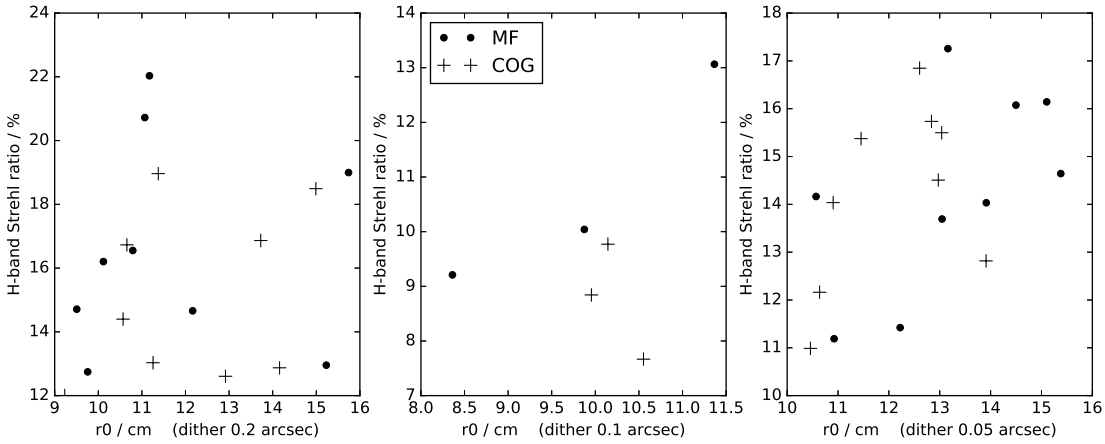

Figure 8. A figure showing AO performance (H-band Strehl) for different closed-loop data sets measured on the night of 19th September using matched filtering and COG algorithms, as a function of Fried's parameter. The mean of these measurements are given in table 1. In this case, the science target has an apparent magnitude of 8.98 and a 3 s exposure is used. The matched filter, and reference slopes for both COG and matched filter were recorded immediately before the start of each dataset. The dither amplitude used to create the matched filter is, from left to right, 0.2 arcseconds, 0.1 arcseconds and 0.05 arcseconds.

surements of the LGS photon return and other experiments. p. 84501R

Conan R., Lardière O., Herriot G., Bradley C., Jackson K., 2009, AO, 48, 1198

Foy R., Labeyrie A., 1985, A&A, 152, L29

Fusco T., Rousset G., Sauvage J. F., Petit C., Beuzit J. L. Dohlen K., Mouillet D., Charton J., Nicolle M., Kasper M., Baudoz P., Puget P., 2006, Opt. Express, 14, 7515

Gach J.-L., Feautrier P., Buey T., Rousset G., Gendron E., Morris T. J., Basden A., Stadler E., Myers E., Vidal F., Chemla F., 2016, in Gavel D., Trancho G., eds, Proceedings of the Fourth AO4ELT Conference OCAM2S: an integral shutter ultrafast and low noise wavefront sensor camera for laser guide stars adaptive optics systems. p. 58

Gendron E., Vidal F., Brangier M., Morris T., Hubert Z., Basden A. G., Rousset G., Myers R., 2011, A&A, 529, L2

Gilles L., Ellerbroek B., 2006, AO, 45, 6568

Gilles L., Ellerbroek B. L., 2008, Optics Letters, 33, 1159

Gordon J. A., Buscher D. F., Baron F., 2011, Appl. Opt., 50, 5303

Hammer F., Barbuy B., Cuby J., Kaper L., Morris S., Evans C., Jagourel P., Puech M., 2014, in Society of Photo-Optical Instrumentation Engineers (SPIE) Conference Series Vol. in print of Society of Photo-Optical Instrumentation Engineers (SPIE) Conference Series, MOSAIC at E-ELT: a MOS for astrophysics, IGM, and cosmology

Jovanovic N., Martinache F., Guyon O., Clergeon C. e. a., 2015, Pub. Astron. Soc. Pacific, 127, 890

Macintosh B. A., Anthony A., Atwood J., Barriga N., Bauman B., Caputa K., Chilcote J., Dillon D., Doyon R., Dunn J., Gavel D. T., Galvez R., Goodsell S. J., 2012, in Society of Photo-Optical Instrumentation Engineers (SPIE) Conference Series Vol. 8446 of Society of Photo-Optical Instrumentation Engineers (SPIE) Conference Series, The Gemini Planet Imager: integration and status

Moussaoui N., Clemesha B. R., Holzlöhner R., Simonich D. M., Bonaccini Calia D., Hackenberg W., Batista P. P., 2010, A&A, 511, A31

Myers R. M., Hubert Z., Morris T. J., Gendron E., Dipper N. A., Kellerer A., Goodsell S. J., Rousset G., Younger E., Marteaud M., Basden A. G., 2008, in Society of Photo-Optical Instrumentation Engineers (SPIE) Conference Series Vol. 7015 of Presented at the Society of Photo-Optical Instrumentation Engineers (SPIE) Conference, CANARY: the on-sky NGS/LGS MOAO demonstrator for EAGLE

Nelson J., Sanders G. H., 2008, in Society of Photo-Optical Instrumentation Engineers (SPIE) Conference Series Vol. 7012 of Society of Photo-Optical Instrumentation Engineers (SPIE) Conference Series, The status of the Thirty Meter Telescope project. pp 70121A–70121A–18

Osborn J., Wilson R., Butterley T., Shepherd H., Sarazin M., 2010, MNRAS, 406, 1405

Rigaut F., Neichel B., Boccas M., d'Orgeville C., Arriagada G., Fesquet V., Diggs S. J., Marchant C., Gausach G., Rambold W. N., Luhrs J., Walker S., Carrasco-Damele E. R., Edwards M. L., Pessev P., Galvez R. L., 2012, in Society of Photo-Optical Instrumentation Engineers (SPIE) Conference Series Vol. 8447 of Society of Photo-Optical Instrumentation Engineers (SPIE) Conference Series, GeMS: first on-sky results

Rousset G., Gratadour D., Gendron E., Buey T., Myers R., Morris T., Basden A. G., Talbot G., Bonaccini Calia D., Marchetti E., Pfrommer T., 2014, in Society of Photo-Optical Instrumentation Engineers (SPIE) Conference Series Vol. 9148 of Society of Photo-Optical Instrumentation Engineers (SPIE) Conference Series, Proposal for a field experiment of elongated Na LGS wave-front sensing in the perspective of the E-ELT. p. 3

Sarazin M., Le Louarn M., Ascenso J., Lombardi G., Navarrete J., 2013, in Adaptative Optics for Extremely Large Telescopes 3 Defining reference turbulence profiles for E-ELT AO performance simulations

Tamai R., Spyromilio J., 2014 Vol. 9145, European ex-

tremely large telescope: progress report. pp 91451E–91451E–9
Thomas S., Fusco T., Tokovinin A., Nicolle M., Michau V., Rousset G., 2006, MNRAS, 371, 323
Vidal F., Gendron É., Rousset G., Morris T., Basden A., Myers R., Brangier M., Chemla F., Dipper N., Gratadour D., Henry D., Hubert Z., Longmore A., Martin O., Talbot G., Younger E., 2014, A&A, 569, A16

This paper has been typeset from a TEX/ LATEX file prepared by the author.